

# Characterizing Femtosecond Laser Tagging Performance with a 1030 nm Yb:KGW Laser and Application to Continuous 50 kHz Velocimetry

Weixiao Wang<sup>1</sup>, Rishav Choudhary<sup>2</sup>, Christopher M. Limbach<sup>3,\*</sup>

1 : Graduate Researcher, Department of Aerospace Engineering, University of Michigan, Ann Arbor

2 : Postdoctoral Fellow, Department of Aerospace Engineering, University of Michigan, Ann Arbor

3 : Assistant Professor, Department of Aerospace Engineering, University of Michigan, Ann Arbor

\*Corresponding author: [limbach@umich.edu](mailto:limbach@umich.edu)

**Keywords:** High-Speed Velocimetry

## ABSTRACT

This paper presents a comprehensive evaluation of unseeded Femtosecond Laser Electronic Excitation Tagging (FLEET) using a 1030 nm Yb:KGW femtosecond laser. In the first part of this work, fundamental studies were conducted in a vacuum chamber to assess the fluorescence process in dry air and nitrogen. Specifically, the effects of pressure, pulse energy, and focal length on the temporal decay of the nitrogen first and second positive band emission are quantified and reported. The results show similar trends to previous reports of FLEET emission behavior at other visible and near infra-red excitation wavelengths, indicating that the same fundamental fluorescence mechanism occurs after 1030 nm excitation. In the second part of this work, we explore the application of 1030 nm FLEET to continuous high-speed velocimetry in an under-expanded laboratory jet. Unseeded velocity measurements at 50 kHz in air were acquired at several points in the flow using burst gating of a high-speed intensifier. Frequency domain analysis of over 50,000 time-resolved measurements show strong periodic fluctuations near 8 kHz due to an acoustic resonance near the jet exit. Analysis of the streamwise velocity autocorrelation is shown to provide a means to separate uncorrelated random measurement error from true flow fluctuations. These results establish a first demonstration of continuous, high-speed FLEET measurements at 1030 nm and provides foundational data to inform future applications of this unseeded velocimetry technique in turbulent high-speed flows.

---

## 1. Introduction

Optical diagnostics based on spectroscopy, molecular/atomic tagging, particle tracking, and laser interference have shown great capability and potential for improving our understanding of reacting and non-reacting flows. Their non-intrusive nature allows for precise measurements of flow variables with a high spatial and temporal resolution. In the context of velocimetry, particle-based techniques such as Particle Image Velocimetry (PIV) have proven exceptionally powerful. However, the finite relaxation time of particles in high acceleration zones, such as shocks, limit applications of PIV to supersonic and hypersonic flows [Williams et al. (2015), Sakurai et al. (2015)].

Instead, Molecular Tagging Velocimetry (MTV) has demonstrated significant advantages by tracking molecular species which respond very quickly to the flow dynamics. Different molecular tagging velocimetry techniques target specific electronic transitions, or photolytic processes, in gas molecules. For example, the Raman Excitation Plus Laser-Induced Electronic Fluorescence (RELIEF) technique tags and tracks molecular oxygen through vibrational pumping, while Air Photolysis and Recombination Tracking (APART) employs a UV laser to dissociate oxygen and form nitric oxide, which is then tracked by Laser-Induced Fluorescence (LIF) [Michael et al. (2011), Peters et al. (2015)].

The current work focuses on MTV using femtosecond (fs) laser pulses that provide non-resonant excitation of the test gas, typically nitrogen or air. The molecules within the excitation region undergo dissociation, forming atomic nitrogen, which recombines into the molecular nitrogen  $B$  state manifold. These molecules produce fluorescence that persists for tens of microseconds [Michael et al. (2011), Peters et al. (2015)] during which time the fluorescing species are convected by the flow. Known as Femtosecond Laser Electronic Excitation Tagging (FLEET), this method uniquely targets the fluorescence from the dissociation and recombination of molecular nitrogen, providing a means to track the motion of the molecules by monitoring the displacement of these tagged molecules through a time-delayed, fast-gated camera [Peters et al. (2015)]. By measuring the distance traveled over a predetermined time delay, this velocimetry technique allows for the accurate determination of the local flow velocity.

FLEET velocimetry was first studied and demonstrated by Micheal et al. at Princeton University [Michael et al. (2011)]. Subsequent research has expanded and deepened the understanding of this velocimetry technique in several important aspects. This includes two-dimensional velocity and vorticity measurements achieved by tagging two perpendicular FLEET lines [N. D. Calvert et al. (2014)], the determination of measurement precision using high-speed complementary metal-oxide semiconductor (CMOS) cameras [Peters et al. (2015)], and the assessment of heating and gas perturbations caused by the femtosecond laser-induced plasma [Limbach & Miles (2017)]. Additional studies have explored the relationship of FLEET signals with different gas mixtures [N. Calvert et al. (2016), Zhang et al. (2017), Zhang et al. (2018)], the effects of laser pulse energy and spectra on FLEET signals [DeLuca et al. (2014)], and the impacts of temperature and pressure on these signals [Peters et al. (2020)].

Owing to the simplicity of its setup, which requires only a single femtosecond laser system paired with a high-speed intensified CMOS or CCD camera, FLEET has been widely applied in numerous environments. These applications range from the characterization of high-speed turbulent flows in ground-test facilities [Dogariu et al. (2019)], to the determination of the state and velocity profile of turbulent compressible boundary layers in hypersonic flow [Dogariu et al. (2019), Hill et al. (2021), Pehrson, Leonov, Melone, et al. (2023), Pehrson, Leonov, Miles, et al. (2023)], and in reacting flows [Murray et al. (2018), Li et al. (2019)].

At present, continuous FLEET measurements have been undertaken with Ti:Sapphire laser technology at acquisition rates on the order of 1-10 kHz. Higher repetition rates have been achieved using custom burst-mode femtosecond and picosecond lasers, with 1 MHz rates demonstrated over a 0.5 ms long burst [Fisher et al. (2020)]. While these burst-mode systems are well-suited to investigating coherent structures in impulse facilities, their sampling duration limits the size of the statistical sample, constraining the study of power spectra, velocity correlations, and correlations with other flow variables such as density and temperature that relate to the Reynolds stress and turbulent heat flux. These limitations highlight the need for continuous, high repetition rate MTV methods to better capture statistical metrics of turbulence in high-speed flows.

To address this need, this current work investigates using a Yb:KGW femtosecond laser with 1030 nm wavelength to perform FLEET velocimetry. Unlike Ti:Sapphire, the Yb:KGW gain medium permits diode pumping, resulting in a smaller form factor, and improved thermal properties that facilitate power scaling. However, the gain bandwidth is somewhat narrower than Ti:Sapphire, resulting in typical pulse durations near 200 fs. Moreover, FLEET tagging at 1030 nm occurs through a 13-photon ionization process rather than the 11-photon process at 800 nm. To investigate these differences and their effect on FLEET velocimetry, here we present a first characterization of the nature of the fluorescence associated with non-resonant excitation at 1030 nm with a 200 fs pulse duration. In particular, this work explores the FLEET signal dependence on parameters such as pressure, gas composition (air or nitrogen), pulse energy, and lens focal length.

## 2. Experimental Setup and Methods

The experiments presented here were conducted using a Light Conversion PHAROS Femtosecond Laser System as the excitation source. This laser features a center wavelength of 1030 nm and 8 nm bandwidth, with a maximum average power of 20 W. The repetition rate can be varied from single shot to 200 kHz, and the unfocused beam diameter is  $6.6 \pm 0.7$  mm. A maximum pulse energy of 4 mJ can be obtained at repetition rates of 5 kHz or less, with pulse-to-pulse energy variation and long-term output power variation of less than 0.5 %.

The characterization of the FLEET emission is performed under nearly static flow conditions generated in a low-pressure gas cell, as shown in Figure 1. Gas inlets allow a steady flow to be generated. This is crucial to prevent the build-up of contaminant gas species which we have observed can affect the FLEET signal due to differences in excitation and energy exchange with impurities [Peters et al. (2015), Limbach & Miles (2017), Peters et al. (2020)].

The low-pressure cell consists of a spherical octagon, featuring two 6 inch ConFlat (CF) flange ports on the top and bottom and eight 2.75 inch CF flange ports on the side. A Kodial glass viewport provides optical access from the side for signal collection, while two side-ports which pass the fs beam are fitted with laser-grade 1 inch diameter windows with anti-reflection coatings.

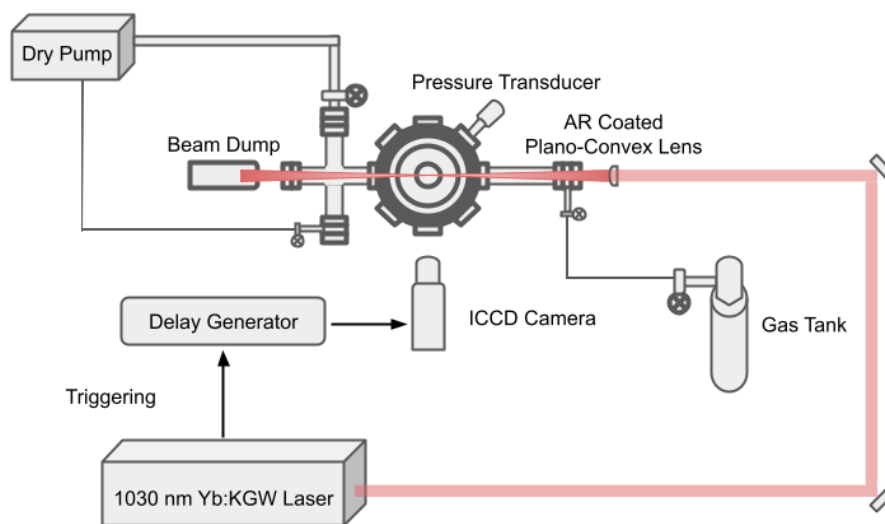


**Figure 1.** Schematic of the static, low pressure femtosecond laser excitation experiment

During fluorescence imaging experiments, the background was kept dark to prevent corruption of the signal by stray reflections, while during calibration, a white screen was illuminated by a white light source to provide a spatial calibration of the optical system throughput. The imaging system consisted of an Andor iStar Intensified-CCD (DH734-25F-03) Camera with Nikon 105mm f/2.8 FX AF Micro-Nikkor Lens. The imaging system configuration was held constant during all characterization processes to provide a consistent comparison between data collected at different conditions. To field of view was chosen to provide full imaging of the longest and widest emission profile, resulting in an image scale of 50 microns per pixel. Notably, this resolution is comparable to the beam waist determined from Gaussian optics.

During experiments, the laser was focused into the cell through the axially oriented viewports. To avoid laser damage on the entry and exit windows, two 125 mm long CF nipples were introduced on opposite sides of the chamber to increase the standoff distance. Several plano-convex lenses (AR coated for 700-1100 nm) with different focal length including 150mm, 300mm, 500mm, and 1000 mm were used for focusing the beam. The pressure was monitored using an Inficon Pirani Capacitance Diaphragm Gauge (PCG55x) pressure transducer. A pair of NPT ports served as a gas inlet and outlet, with a slow flow oriented axially with the laser. Prior to each experiment, the cell was evacuated using a dry scroll vacuum pump (Ebara EV-SA20) to an ultimate pressure of 1 mTorr. Following this, the gas inlet and outlet valves were adjusted to achieve a steady flow of the gas at the desired pressure. To change the cell pressure, the gas inlet pressure was adjusted, along with the set point of the inlet and outlet valves.

Static fs laser excitation experiments were conducted with ultra pure nitrogen or dry air. The repetition rate of the laser was kept fixed at 1 kHz, both to allow for test gas refreshing and in keeping with previous literature, while the pressure, pulse energy, and intensity of focusing were varied.

The camera gating was synchronized with the laser pulse and delayed by various amounts while the exposure time was selected depending on the specific conditions to prevent signal saturation in the images and maximize the signal to noise ratio. The camera gate width and gain were kept fixed at 200 ns and 100, respectively. On-chip integration was further utilized to accumulate all signals collected during the exposure period with the intensifier gain was held constant for all experiments.

### 3. Results and Discussion

#### 3.1. Analysis with Different Pulse Energies

First we present and analyze the spatial profile of the FLEET signal obtained by focusing with a 300 mm lens into 10 Torr of nitrogen with varying pulse energy. Images of the fluorescence profile are shown in Figure 2.

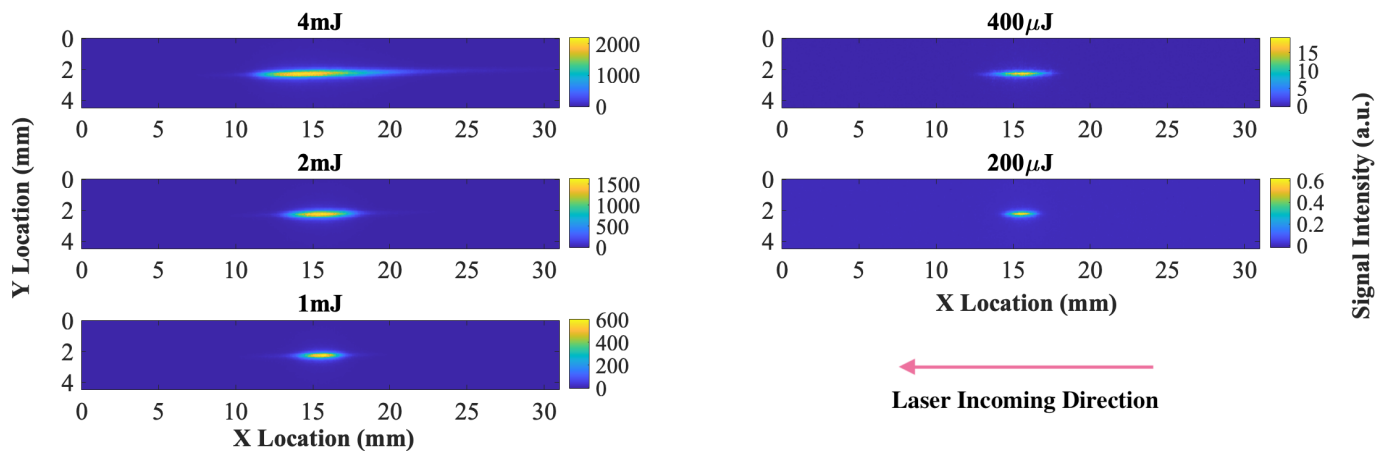


**Figure 2.** FLEET images obtained with different pulse energies at 0.1  $\mu s$  delay and 300 mm focal length lens in nitrogen at 10 Torr.

A typical trend of increasing fluorescence length is observed with increased laser power. Several different quantitative metrics of the fluorescence morphology are presented in Table 1, which also includes the intensity of a focused laser pulse ( $I$ ) and the Rayleigh length ( $z_R$ ). The length metrics reports include the horizontal and vertical lengths of the tagged region ( $L_x$  and  $L_y$ ), the square root of the central second moment ( $\sqrt{\text{Var}(x)}$  and  $\sqrt{\text{Var}(y)}$ ), and standard deviation for a 2D Gaussian fit ( $\sigma_x$  and  $\sigma_y$ ). Here, the tagged region is defined as the area over which the pixel intensities at least twice the standard deviation of the background noise. The central second moment of the distribution, or variance, was calculated along with the Gaussian function fit width to quantify the spatial spread of the distribution around the centroid.

**Table 1.** Laser pulse and emission profile parameters obtained with 300 mm focusing as a function of pulse energy.

Pulse Energy (mJ)	I (W/cm <sup>2</sup> )	z <sub>R</sub> (mm)	L <sub>x</sub> (mm)	L <sub>y</sub> (mm)	$\sqrt{\text{Var}(x)}$ (mm)	$\sqrt{\text{Var}(y)}$ (mm)	$\sigma_x$ (mm)	$\sigma_y$ (mm)
4	$7.17 \times 10^{14}$	2.71	13.85	1.25	2.42	0.19	2.54	0.19
2	$3.58 \times 10^{14}$	2.71	7.00	1.30	1.20	0.19	1.34	0.17
1	$1.79 \times 10^{14}$	2.71	6.05	1.30	0.88	0.18	0.90	0.15
0.4	$7.17 \times 10^{13}$	2.71	5.65	1.30	0.99	0.17	1.04	0.13
0.2	$3.58 \times 10^{13}$	2.71	3.20	1.35	0.56	0.17	0.60	0.13

In Figure 2, we observe that the emission region extends over a length from 3.2 mm to 13.85 mm and at high pulse energy exhibits a notable asymmetry, with higher emission on the side of the focus closer to the focusing lens. This effect is consistent with incipient self-focusing and filamentation observed in other FLEET experiments [DeLuca et al. (2014)]. The asymmetry at high energy is more clearly visible when plotting the horizontal intensity profile, as shown in Figure 3. The profiles clearly exhibit symmetry below 2 mJ where beam propagation occurs in the linear regime.

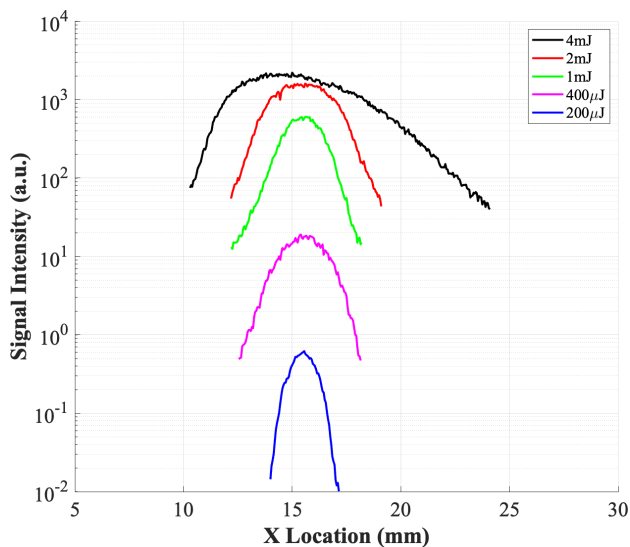


**Figure 3.** Horizontal intensity profiles of the tagged region with 300 mm focusing and different pulse energies.

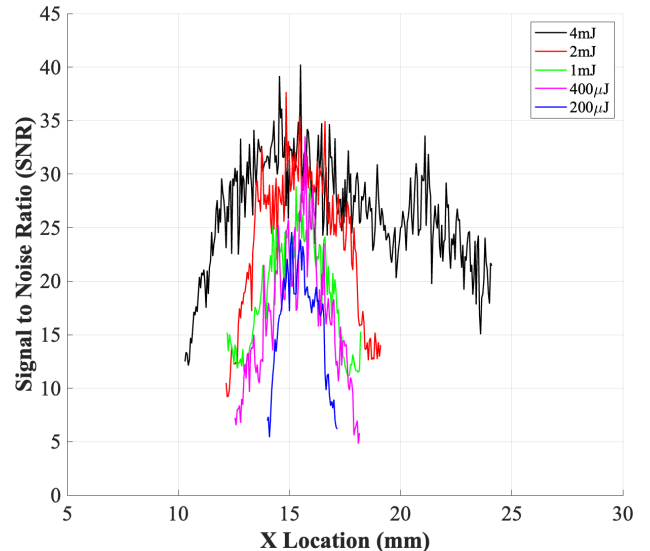


**Figure 4.** Signal to Noise Ratio (SNR) of the tagged region with 300 mm focusing and different pulse energies.

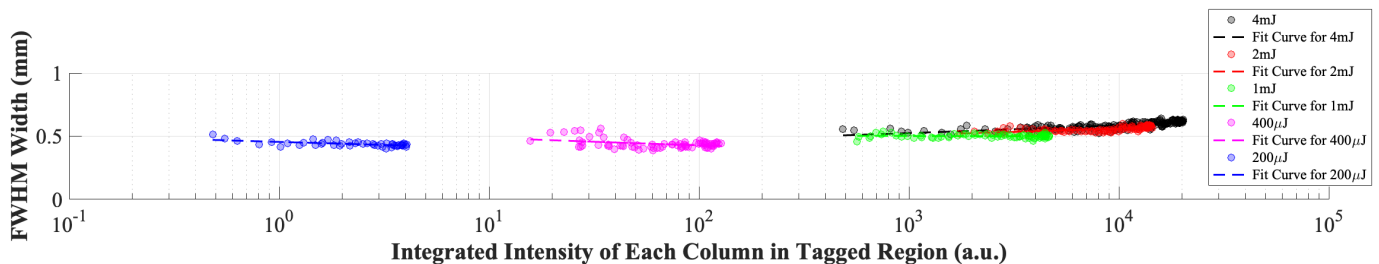


**Figure 5.** Relationship between FWHM and intensity in the tagged region with different pulse energies

To quantify signal levels we compute the Signal-to-Noise Ratio (SNR) by dividing the Gaussian fit peak by the root-mean-square deviation (RMSD) of the residual obtained by subtracting the real data and Gaussian fit. The results, shown in Figure 4, indicate that higher pulse energies yield about 60% higher SNR on line center compared with the lower energy case. The SNR profile shape within the tagged region mirrors the horizontal intensity profile at the weighted centroid location, demonstrating that signal intensity significantly influences SNR values. Note, however, that the reported SNR pertains to averaged rather than signal shot data and primarily informs the quality of other time-averaged results presented herein.

Additionally, Figure 5 analyzes the correlation between FWHM values and the total intensity for a delay of 0.1  $\mu$ s. To create this plot, the peak intensity and width of the column-wise Gaussian fits were plotted against one another, with a linear fit shown for each dataset to provide a guide for the eye. This data shows a significant but nonlinear correlation between the FLEET intensity and line width at higher pulse energies ( $\geq 2$  mJ), while at lower pulse energies ( $< 2$  mJ), there appears to be no obvious correlation. This finding is consistent with previous measurements [Limbach & Miles (2017), Limbach (2015)] that attributed increasing FLEET line width to gas heating, partially due to hot, electronically excited N atom production. Unlike previous results with Ti:Sapphire lasers [DeLuca et al. (2014)], we find only a small change in the fluorescence line width at the highest energy, suggesting that the energy deposition using the 1030 nm laser, under these conditions, may not be too severe. However, we caution that further work is needed to quantify gas heating for this FLEET excitation scheme.

### 3.2. Effect of Focusing

Next, we present and analyze the spatial profile of the FLEET signal obtained with different focusing strengths at 10 Torr, with a 2 mJ pulse energy and nitrogen as the test gas. First, we present imaging of the FLEET emission profile in Figure 6 and quantitative width metrics in Table 2.

**Table 2.** Spatial profile metrics as a function of laser focusing.

Focal Length (mm)	I (W/cm <sup>2</sup> )	$z_R$ (mm)	$L_x$ (mm)	$L_y$ (mm)	$\sqrt{\text{Var}(x)}$ (mm)	$\sqrt{\text{Var}(y)}$ (mm)	$\sigma_x$ (mm)	$\sigma_y$ (mm)
1000	$3.23 \times 10^{13}$	30.11	28.70	1.20	6.22	0.18	6.95	0.19
500	$1.29 \times 10^{14}$	7.53	18.95	1.15	3.00	0.16	2.83	0.16
300	$3.58 \times 10^{14}$	2.71	7.00	1.30	1.20	0.19	1.34	0.17
150	$1.43 \times 10^{15}$	0.68	4.45	1.40	0.83	0.21	0.95	0.20

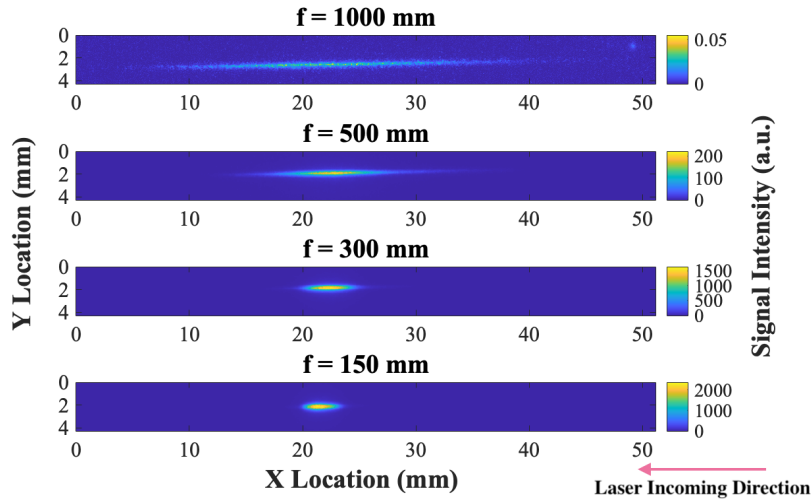


**Figure 6.** FLEET images obtained with different focusing parameters at a  $0.1 \mu\text{s}$  delay and 2 mJ pulse energy in 10 Torr nitrogen.

We observed that, with different focusing strength, the width of the FLEET tagged region does not vary significantly when changing the focal length but keeping pulse energy fixed. Notably, the larger vertical width seen at a focal length of 1000 mm may be attributed to resolving the beam waist, which we estimate using to be  $2w_0 = 0.20 \text{ mm}$  using Gaussian optics. In the direction of laser propagation the length varies considerably, consistent with previous findings.

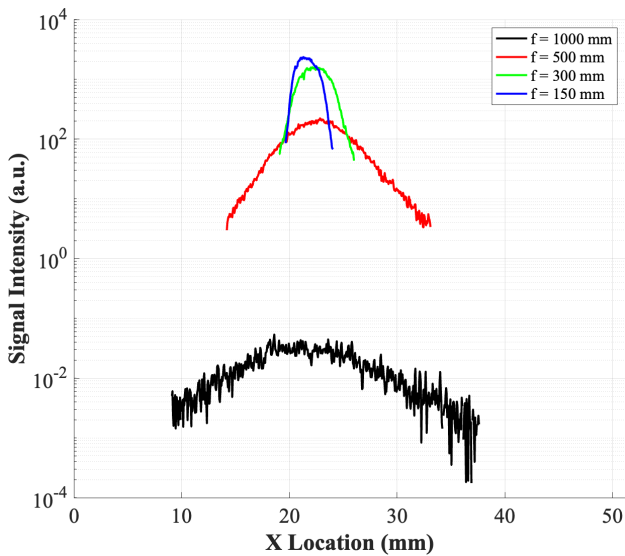


**Figure 7.** Horizontal intensity profiles of the tagged region with 2 mJ pulse energy and different focal length lenses.

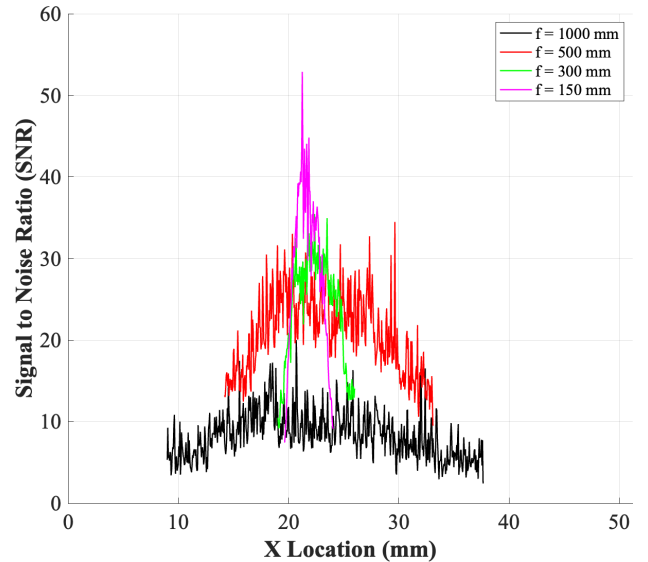


**Figure 8.** Signal to Noise Ratio (SNR) of the tagged region with 2 mJ pulse energy and different focal length lenses.

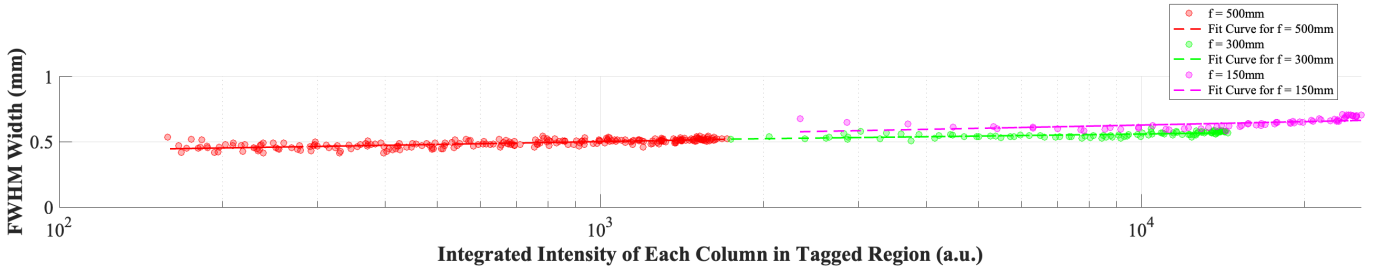


**Figure 9.** Relationship between FWHM and intensity in the tagged region with different focal length lenses.

In Figure 7, the intensity profile exhibits several orders of magnitude difference depending on the degree of focusing, consistent with the highly nonlinear nature of the excitation process. As seen before for pulse energy variation, shorter focal lengths yield higher emission intensity, resulting in a significant increase in SNR values as seen in Figure 8. Figure 9 presents the column-wise correlation between FLEET intensity and line width for focal lengths, with the 1000 mm case excluded based on the presence of significant noise. Interestingly, we observe that the width correlates with the emission intensity, rather than the lens focal length, providing further evidence that heat release dominates the emission width rather than the laser beam width.

### 3.3. Trends with Pressure and Delay

Next, we consider the variation in signal as a function of gas pressure and time delay. These trends are captured in Figure 10 with nitrogen and Figure 11 with dry air. This dataset spans a pressure range from 1 Torr to 760 Torr and an initial time delay range from 0.1  $\mu\text{s}$  to 100  $\mu\text{s}$ . This range of parameters is particularly relevant to flow tagging applications in wind tunnels at velocities  $\gtrsim 10$  m/s.

The observed pressure dependence of the signal shows a characteristic dip at intermediate sub-atmospheric pressures, with the minimum signal depending on the particular delay. At the shortest delay measured here (0.1  $\mu\text{s}$ ), the minimum signal occurs near 500 Torr in both air and nitrogen. At the longest delays, the minimum signal shifts to progressively lower pressure, with signals no longer detectable below 20 Torr and delays longer than 25  $\mu\text{s}$ . Previous investigations have attributed these trends to an interplay between density (which increases N atom yield and signal), diffusion, and quenching [Leonov et al. (2012), DeLuca et al. (2014)]. Counter-intuitively, signal can increase at very low pressure due to the reduction in quenching, however the peak signal decays quickly due to diffusion of N atoms, leading to a reduced three-body recombination rate. A subset of data illustrating these effects can be seen in Figure 12, which shows that despite an initial decay that appears similar in all cases, the long-time behavior is governed by pressure rather than gas composition. Qualitatively, these results are similar to previous reports [Peters et al. (2020)], wherein FLEET emission in nitrogen exhibits an order of magnitude higher signal than in dry air.

Notably, the similarity between the results presented here and previous reports offers strong evidence that the underlying fluorescence mechanism is no different at 1030 nm than other visible and near-IR excitation wavelengths.

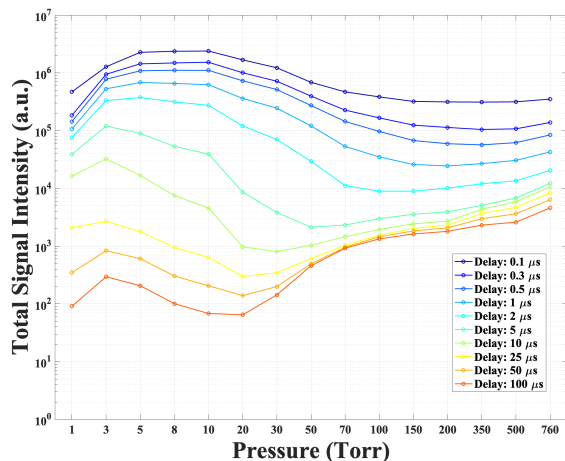


**Figure 10.** Total signal intensity in tagged region vs. pressures at different time delay at 4mJ pulse energy with 300 mm focal length lens in nitrogen.

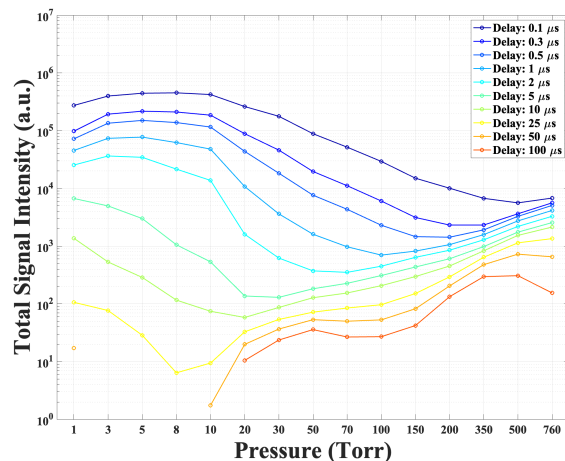


**Figure 11.** Total signal intensity in tagged region vs. pressures at different time delay at 4mJ pulse energy with 300 mm focal length lens in dry air.

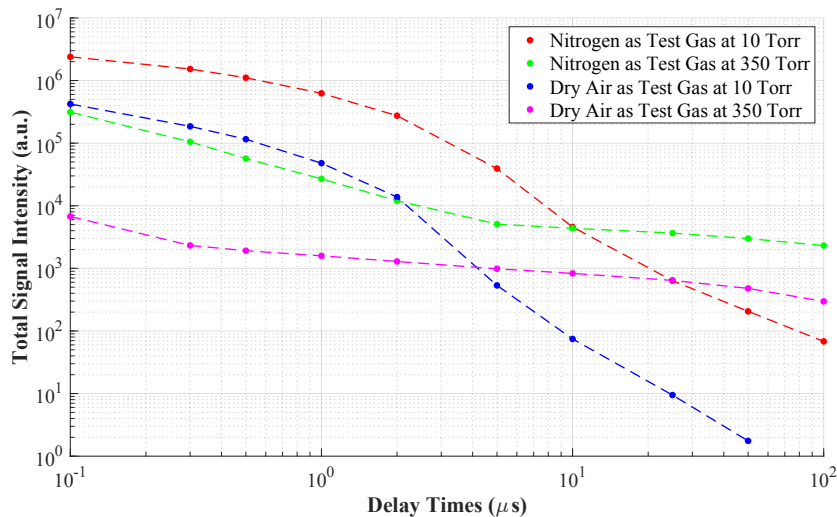


**Figure 12.** Signal intensity decay with nitrogen or dry air at 350 Torr and 10 Torr.

#### 4. FLEET Experiments at 50 kHz Repetition Rate

The characterization of FLEET emission presented in Section 3 allows for estimation of signal levels obtained with various pulse energy and focusing combinations. To achieve high sampling rates,

our initial efforts have aimed to demonstrate sufficient speed to capture correlations in the fluctuating velocity which could be used to characterize key features of unsteady flows. As described in this section, measurement rates of 50 kHz have been achieved with  $400 \mu\text{J}$  per pulse and focusing by a 100 mm lens. What follows is a description of the experimental setup and key results.

For this investigation, an underexpanded jet of dry air was generated by a 0.29" diameter orifice was used as the test-bed for demonstrating high-speed FLEET velocimetry. The orifice was bored out on a stainless steel flange and consisted of a step change in area from 3 inches to 0.29 inches. The length of the 0.29 inch diameter constriction 0.1 inches. The 3 inch diameter face was connected to a compressed air supply through a reducing nipple and a pressure gauge downstream of the nipple was used for determining the stagnation pressure of the flow. All experiments presented here were conducted at a stagnation pressure of 80 psia.

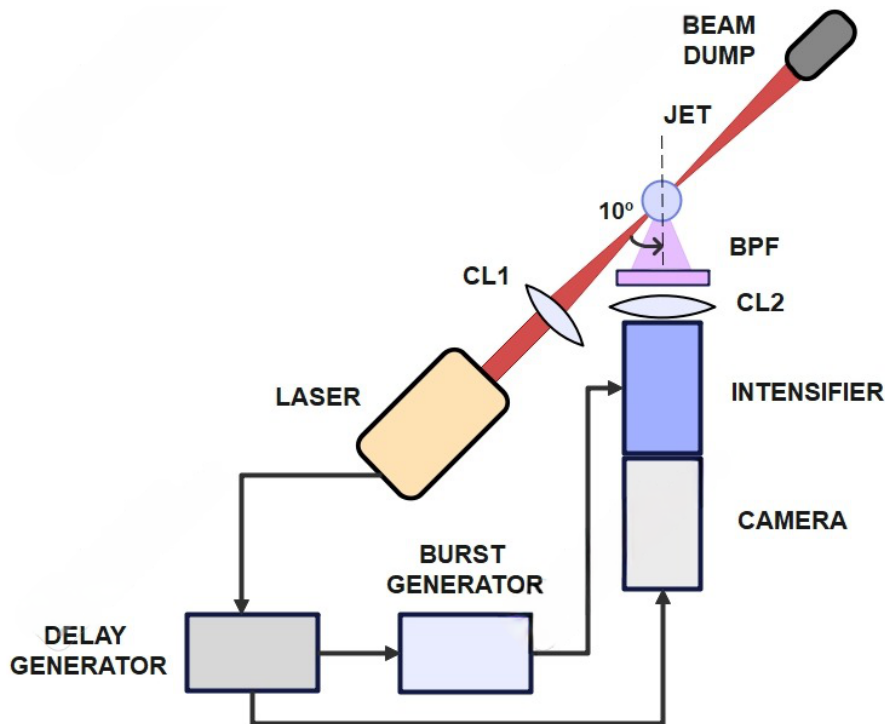


**Figure 13.** Schematic of the FLEET velocimetry setup. Note that the angle between the laser line-of-sight, and the detection axis is exaggerated. (CL: Convex Lens, BPF: Bandpass Filter)

A schematic of the experimental setup is shown in Figure 13. The velocimetry laser was focused on the axis of the jet using a 100 mm focal length AR coated plano-convex lens. Guided by the characterization discussed in the previous section, the pulse energy of the laser was set to  $400 \mu\text{J}$ , the maximum possible for a 50 kHz rate. Owing to the spatial constraints, the fluorescence was recorded at an angle of 10 degrees from the line of sight of the incident laser. A CMOS camera (Phantom v711) was used to record the fluorescence signal. The frame rate of the camera and the exposure time were set to 50 kHz and  $20 \mu\text{s}$ , respectively. A UV intensifier, LaVision HS-IRO, was

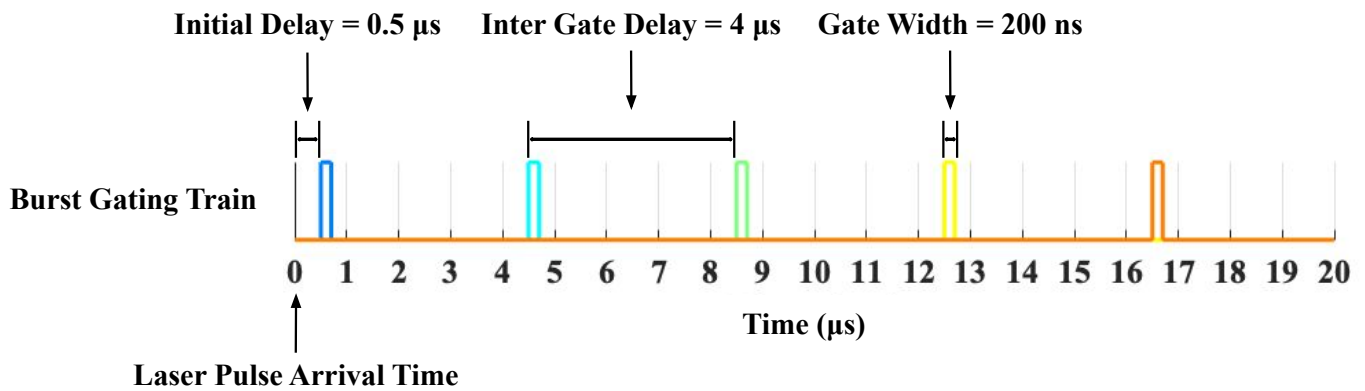


**Figure 14.** Timing diagram of burst gating for FLEET experiments at 50 kHz rate

used for amplifying the weak fluorescence signal from the FLEET filament before being recorded by the CMOS camera. A broadband low-pass filter with a 950 nm cutoff was placed in front of the intensifier to permit light in the UV and visible to pass through while rejecting stray light at 1030 nm. The intensifier was configured for burst gating with five pulses starting at a delay of  $0.5 \mu\text{s}$  from the arrival of the laser pulse, as shown in Figure 14. The gate width was set to 200 ns while the inter-gate delay was set to  $4 \mu\text{s}$ , covering completely the total  $20 \mu\text{s}$  between laser pulses. A long exposure photograph of the jet exit and FLEET line is shown in Figure 15, as captured by an iPhone 13 mini. A separate interferometry diagnostic was also present to measure the density field within the jet simultaneously with FLEET velocimetry. While this diagnostic will not be described in detail, visualization of the flowfield will be used to contextualize the FLEET results.

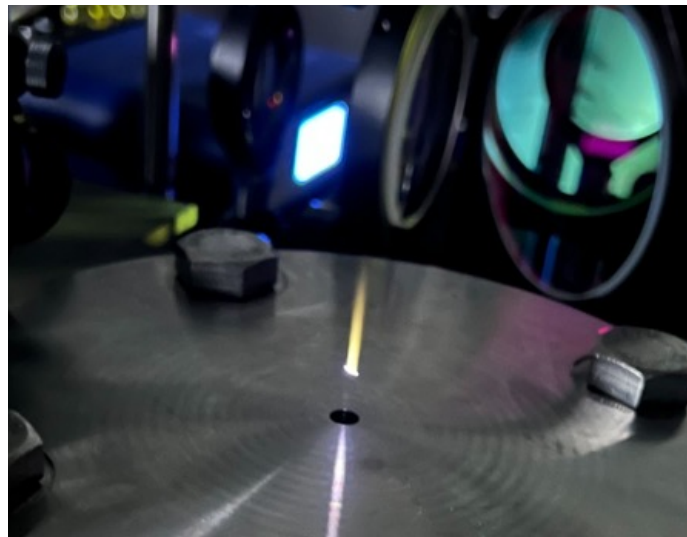


**Figure 15.** Long exposure image of the FLEET emission captured by a smartphone.

Using the burst gating as described above, five distinct regions of fluorescence were recorded on a single image frame, allowing for four distinct measurement locations to be identified. The dis-

tance travelled between two consecutive gating events was used to determine the local velocity of the flow at the respective intermediate locations. Figure 16 shows one of the frames from the FLEET measurements along with the time averaged phase/density measurements from interferometry. Here, red and yellow regions indicate a higher density compared to purple regions. The intermediate locations (numbered 1-4) at which the velocities are determined are labelled on the corresponding density image. Point 1 lies downstream of a Mach disc, while point 4 appears in a downstream shock crossing location. By contrast, points 2 & 3 lie in a rarefaction region. The processed velocity time history at all four locations is shown in the top panel of Figure 17. The velocity is smallest at location 1, as might be expected after a normal shock. It then rises and remains nearly constant at locations 2 and 3 due to the flow acceleration. At location 4, the velocity is then slightly reduced by the crossing shocks.

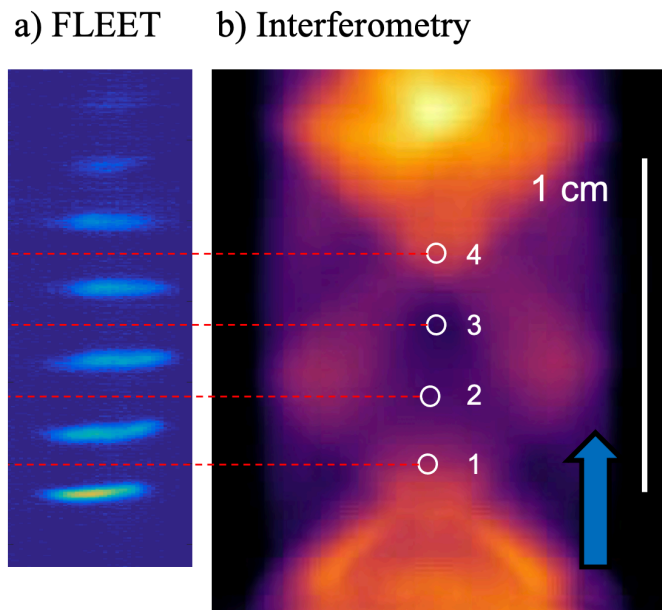


**Figure 16.** Spatial location of FLEET within the under-expanded jet flow. Note the location of point 1 just behind the Mach disc.

The auto-correlation and the power spectrum of the velocity fluctuations at location 1 is shown in middle and bottom panels of Figure 17. The auto-correlation is largest near zero lag and decays with time as would be expected. However, a very strong oscillation is observed at a frequency of nearly 8 kHz. This roughly corresponds to the frequency at which the Mach disc was observed to oscillate and can be attributed to screech.

One significant advantage of the continuous high measurement rate is the ability to separate random and systematic errors in the velocity fluctuation measurement using converged flow statistics. Earlier works using FLEET looked at quantifying the random error for instantaneous measurements using the freestream as a fluctuation-free reference [Pehrson, Leonov, Melone, et al.

(2023), Pehrson, Leonov, Miles, et al. (2023)]. However, this technique is limited because the SNR in the freestream may be different from the region of interest, and in some cases data in a low-fluctuation region may not be available. Instead, we present here an alternative method for separating the physical velocity fluctuations from random errors. If the random errors and physical velocity fluctuations are uncorrelated and normally distributed their variances add in quadrature as  $\sigma_d^2 = \sigma_r^2 + \sigma_v^2$ , where  $\sigma_d^2$  is the variance observed in the data,  $\sigma_r^2$  is that due to random errors, and  $\sigma_v^2$  is the variance due to velocity fluctuations. However, if the random errors are uncorrelated in time then the true variance of velocity fluctuations can be obtained by extrapolating the auto-correlation at finite lag back to zero lag to obtain  $\sigma_v^2$ , since only physical velocity fluctuations are correlated in time. Using the data from location 1 in Figure 17c as an example, we can see that the intercept at zero lag corresponds to  $\sigma_v^2/\sigma_d^2 = 0.34$ . By this method we can conclude that the true value of  $\langle u'^2 \rangle$  is  $165 \text{ m}^2/\text{s}^2$ , representing only 34% of the measured variance of  $\sigma_d^2 = 484 \text{ m}^2/\text{s}^2$  in the raw velocity fluctuation data.

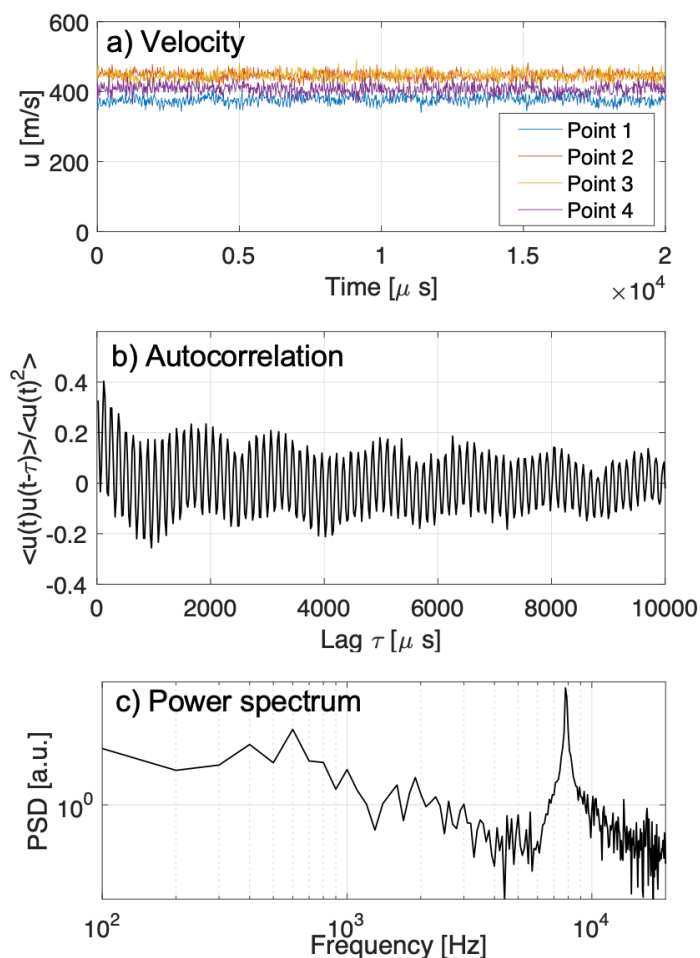


**Figure 17.** a) 50 kHz streamwise velocity measurements. b) Autocorrelation of velocity at point 1. c) Power spectral density of velocity fluctuations at point 1.

The method presented above is not new and has been used with other flow measurements to deduce, for example, integral length scales within turbulent flows. However, this is the first time, to the authors' knowledge, of the technique being applied to molecular tagging velocimetry data in a compressible flow. Currently, this approach to determine fluctuating velocity is limited by the assumptions of Gaussian statistics and uncorrelated noise within the measurement apparatus. There is also a limitation to how accurately the autocorrelation can be extrapolated to zero lag given a finite measurement rate. For this dataset exhibiting the 8 kHz screech, an even higher sampling rate of 100 kHz would further improve the extrapolation accuracy. Both of these considerations are left as the subject of future investigations.

## 5. Conclusions

This work examined the fundamental fluorescence mechanism and trends observed in femtosecond excitation of air with 1030 nm, 200 fs pulses and the capability for continuous high repetition rate velocimetry at 50 kHz. Static measurements showed that FLEET emission signals within the first 2 microseconds are highest at low-pressures below 30 Torr, several magnitudes higher than in the intermediate pressure region near 100 Torr. This finding is particularly relevant and favorable to supersonic and hypersonic wind tunnel testing in the range of static pressures from 2 - 20 Torr. However, a contrasting trend is observed for the FLEET emission signal after 2 microseconds, where the low-pressure region exhibits a faster signal decay compared to the higher pressure region. The qualitative trends are in general agreement with previous investigations of FLEET phenomenology, indicating that the same underlying mechanism is responsible for the observed fluorescence at 1030 nm. High-speed velocimetry was also presented in an under-expanded jet, where 50 kHz measurements were obtained at several locations using a burst gating technique. Analysis of the dataset showed the utility of a large statistical dataset, where an acoustic resonance at 8 kHz was clearly identified from noisy data and extrapolation of the autocorrelation to zero lag was applied to separate random errors and isolate the variance attributable to real velocity fluctuations in the flow.

## 6. Nomenclature

FLEET	Femtosecond Laser Electronic Excitation Tagging
Yb:KGW	Ytterbium-doped Potassium Gadolinium Tungstate
Ti:Sapphire	Titanium:Sapphire
PIV	Particle Image Velocimetry
MTV	Molecular Tagging Velocimetry
RELIEF	Raman Excitation Plus Laser-Induced Electronic Fluorescence
APART	Air Photolysis and Recombination Tracking

UV	Ultraviolet
IR	Infrared
CMOS	Complementary Metal-Oxide Semiconductor
CCD	Charge-Coupled Device
ICCD	Intensified Charge-Coupled Device
a.u.	Arbitrary Unit
CF	ConFlat
f	Focal Length
AR	Anti-Reflection
NPT	National Pipe Thread
I	Intensity ( $\text{W}/\text{cm}^2$ )
$z_R$	Rayleigh Length (mm)
$L_x$	Horizontal Length of the Tagged Region (mm)
$L_y$	Vertical Length of the Tagged Region (mm)
Var(x)	Centered Second Moment of Area (Variance) in Horizontal Direction (mm)
Var(y)	Centered Second Moment of Area (Variance) in Vertical Direction (mm)
$\sigma_x$	Standard Deviation for a 2D Gaussian Distribution in Horizontal Direction (mm)
$\sigma_y$	Standard Deviation for a 2D Gaussian Distribution in Vertical Direction (mm)
$I_i$	Pixel Intensity (a.u.)
$x_i$	Centroid Coordinate of Tagged Region in Horizontal Direction
$y_i$	Centroid Coordinate of Tagged Region in Vertical Direction
A	Amplitude of the Gaussian Fit
FWHM	Full Width Half Maximum
SNR	Signal to Noise Ratio
RMSD	Root Mean Square Deviation
N	Nitrogen Atom
$P_0$	Stagnation Pressure (psi)
$\langle u'^2 \rangle$	Variance in the Velocity Fluctuations ( $\text{m}^2/\text{s}^2$ )

## 7. Acknowledgement

This work was supported, in part, by the Air Force Office of Scientific Research under grant FA9550-20-1-0251 overseen by Dr. Sarah Popkin. We also gratefully acknowledge the support of technicians Thomas Griffin, Terry Larrow, Christopher Chartier, Aaron Borgman, and Doug Barr for their invaluable assistance to this study.

## References

- Calvert, N., Zhang, Y., & Miles, R. B. (2016). Characterizing fleet for aerodynamic measurements in various gas mixtures and non-air environments. In *32nd aiaa aerodynamic measurement technology and ground testing conference* (p. 3206).
- Calvert, N. D., Dogariu, A., & Miles, R. B. (2014). 2-d velocity and vorticity measurements with fleet. In *30th aiaa aerodynamic measurement technology and ground testing conference* (p. 2229).
- DeLuca, N. J., Miles, R. B., Kulatilaka, W. D., Jiang, N., & Gord, J. R. (2014). Femtosecond laser electronic excitation tagging (fleet) fundamental pulse energy and spectral response. In *30th aiaa aerodynamic measurement technology and ground testing conference* (p. 2227).
- Dogariu, L. E., Dogariu, A., Miles, R. B., Smith, M. S., & Marineau, E. C. (2019). Femtosecond laser electronic excitation tagging velocimetry in a large-scale hypersonic facility. *AIAA journal*, *57*(11), 4725–4737.
- Fisher, J. M., Smyser, M. E., Slipchenko, M. N., Roy, S., & Meyer, T. R. (2020). Burst-mode femtosecond laser electronic excitation tagging for khz–mhz seedless velocimetry. *Optics Letters*, *45*(2), 335–338.
- Hill, J. L., Hsu, P. S., Jiang, N., Grib, S. W., Roy, S., Borg, M., . . . Schumaker, S. A. (2021). Hypersonic n 2 boundary layer flow velocity profile measurements using fleet. *Applied Optics*, *60*(15), C38–C46.
- Leonov, S., Firsov, A., Shurupov, M., Michael, J., Shneider, M., Miles, R., & Popov, N. (2012). Femtosecond laser guiding of a high-voltage discharge and the restoration of dielectric strength in air and nitrogen. *Physics of Plasmas*, *19*(12).
- Li, B., Zhang, D., Liu, J., Tian, Y., Gao, Q., & Li, Z. (2019). A review of femtosecond laser-induced emission techniques for combustion and flow field diagnostics. *Applied Sciences*, *9*(9), 1906.
- Limbach, C. M. (2015). *Characterization of nanosecond, femtosecond and dual pulse laser energy deposition in air for flow control and diagnostic applications* (Unpublished doctoral dissertation). Princeton University.
- Limbach, C. M., & Miles, R. B. (2017). Rayleigh scattering measurements of heating and gas perturbations accompanying femtosecond laser tagging. *AIAA Journal*, *55*(1), 112–120.
- Michael, J. B., Edwards, M. R., Dogariu, A., & Miles, R. B. (2011). Femtosecond laser electronic excitation tagging for quantitative velocity imaging in air. *Applied optics*, *50*(26), 5158–5162.

- Murray, T., Fisher, J., Slipchenko, M., & Meyer, T. R. (2018). Femtosecond laser electronic excitation tagging, fleet, for combustion and flow.
- Pehrson, J. C., Leonov, B. S., Melone, K., Lakebrink, M. T., Bowersox, R., Miles, R. B., & Limbach, C. M. (2023). Hypersonic fleet velocimetry and uncertainty characterization in a tripped boundary layer. *Measurement Science and Technology*, 35(1), 015206.
- Pehrson, J. C., Leonov, B. S., Miles, R. B., Lakebrink, M. T., & Limbach, C. (2023). Wall-normal fleet velocimetry in a canonical hypersonic inlet. In *Aiaa scitech 2023 forum* (p. 0220).
- Peters, C. J., Burns, R. A., Miles, R. B., & Danehy, P. M. (2020). Effect of low temperatures and pressures on signal, lifetime, accuracy and precision of femtosecond laser tagging velocimetry. *Measurement Science and Technology*, 32(3), 035202.
- Peters, C. J., Danehy, P. M., Bathel, B. F., Jiang, N., Calvert, N., & Miles, R. B. (2015). Precision of fleet velocimetry using high-speed cmos camera systems. In *31st aiaa aerodynamic measurement technology and ground testing conference* (p. 2565).
- Sakurai, T., Handa, T., Koike, S., Mii, K., & Nakano, A. (2015). Study on the particle traceability in transonic and supersonic flows using molecular tagging velocimetry. *Journal of Visualization*, 18, 511–520.
- Williams, O. J., Nguyen, T., Schreyer, A.-M., & Smits, A. J. (2015). Particle response analysis for particle image velocimetry in supersonic flows. *Physics of Fluids*, 27(7).
- Zhang, Y., Shneider, M. N., & Miles, R. B. (2017). An experimental and theoretical investigation of femtosecond laser excitation in n<sub>2</sub>+ o<sub>2</sub> mixtures. In *33rd aiaa aerodynamic measurement technology and ground testing conference* (p. 3899).
- Zhang, Y., Shneider, M. N., & Miles, R. B. (2018). Femtosecond laser excitation in argon–nitrogen mixtures. *AIAA Journal*, 56(3), 1060–1071.